4602 *Chem. Mater.* **2010,** *22,* 4602–4611
DOI:10.1021/cm1005899

CHEMISTRY OF MATERIALS
Article

Functionalization of UiO-66 Metal−Organic Framework and Highly Cross-Linked Polystyrene with $Cr(CO)_3$: In Situ Formation, Stability, and Photoreactivity

Sachin Chavan,[‡] Jenny G. Vitillo,[‡] Mohammed J. Uddin,[‡,§] Francesca Bonino,[‡] Carlo Lamberti,[‡] Elena Groppo,*[,‡] Karl-Petter Lillerud,[⊥] and Silvia Bordiga[‡]

[‡]*Department of Inorganic, Physical and Material Chemistry, University of Torino, via Giuria 7, 10125 Torino, Italy, and NIS Centre of Excellence and INSTM Reference Center, via Quarello 11, I-10135, Torino, Italy, and* [⊥]*inGAP Centre of Research-Based Innovation Department of Chemistry, University of Oslo, P.O. Box 1033, N-0315 Oslo, Norway.* [§]*Present address: Department of Chemical Engineering & Polymer Science, Shah Jalal University of Science & Technology, SUST, Sylhet-3114, Bangladesh.*

Received February 25, 2010. Revised Manuscript Received May 28, 2010

The formation and stability of (arene)$Cr(CO)_3$ species inside two highly porous materials—UiO-66, which is a recently synthesized metal−organic framework, and a cross-linked poly(styrene-co-divinylbenzene) resin—are investigated in detail by means of complementary spectroscopic techniques and theoretical calculations. In particular, Fourier transform infrared (FT-IR), ultraviolet-visible (UV−vis), and X-ray absorption near-edge structure (XANES) spectroscopies, coupled with theoretical calculations, allow the formation of the (arene)$Cr(CO)_3$ species to be followed in situ, starting from the $Cr(CO)_6$ precursor, monitoring the changes in the vibrational and electronic properties of the materials. EXAFS spectroscopy gives the structural evidence of the functionalized unities. Finally, the photoinduced reactivity of $Cr(CO)_3$ in UiO-66 is also explored, by following the substitution of one CO ligand with a N_2 molecule. The overall presented data would become the starting point for the development of a systematic procedure for investigating functionalized porous matrices.

1. Introduction

Functionalization of metal−organic framework (MOF) materials remains one of the main challenges driving the MOF community,[1−11] even more than the optimization of the synthesis conditions to make always newer and newer structures. Indeed, the metal sites in most of the MOFs structures show, at maximum, one coordination vacancy (and only after removal of the solvent), therefore limiting their application (e.g., in catalysis, where at least two coordination vacancies are required). The postsynthesis introduction of metal moieties in the framework by grafting is one of the strategies followed in the perspective of application of MOF in catalysis.[1,8,9,12−22] Grafting of metal-containing species can occur when the MOF framework shows reacting groups (such as −OH, $-NH_2$, and others); however, this excludes the application of the method in the case of MOFs that do not have functional groups (or have in very small amounts). Another possibility is the direct functionalization of the arene belonging to the organic linkers.

*Author to whom correspondence should be addressed. E-mail: elena.groppo@unito.it.

(1) Goto, Y.; Sato, H.; Shinkai, S.; Sada, K. *J. Am. Chem. Soc.* **2008**, *130*, 14354–14355.
(2) Tanabe, K. K.; Wang, Z. Q.; Cohen, S. M. *J. Am. Chem. Soc.* **2008**, *130*, 8508–8517.
(3) Morris, W.; Doonan, C. J.; Furukawa, H.; Banerjee, R.; Yaghi, O. M. *J. Am. Chem. Soc.* **2008**, *130*, 12626–12627.
(4) Doonan, C. J.; Morris, W.; Furukawa, H.; Yaghi, O. M. *J. Am. Chem. Soc.* **2009**, *131*, 9492–9493.
(5) Yamada, T.; Kitagawa, H. *J. Am. Chem. Soc.* **2009**, *131*, 6312–6313.
(6) Gadzikwa, T.; Farha, O. K.; Mulfort, K. L.; Hupp, J. T.; Nguyen, S. T. *Chem. Commun.* **2009**, 3720–3722.
(7) Gadzikwa, T.; Farha, O. K.; Malliakas, C. D.; Kanatzidis, M. G.; Hupp, J. T.; Nguyen, S. T. *J. Am. Chem. Soc.* **2009**, *131*, 13613–13615.
(8) Qiu, S. L.; Zhu, G. S. *Coord. Chem. Rev.* **2009**, *253*, 2891–2911.
(9) Savonnet, M.; Aguado, S.; Ravon, U.; Bazer-Bachi, D.; Lecocq, V.; Bats, N.; Pinel, C.; Farrusseng, D. *Green Chem.* **2009**, *11*, 1729–1732.
(10) Ingleson, M. J.; Heck, R.; Gould, J. A.; Rosseinsky, M. J. *Inorg. Chem.* **2009**, *48*, 9986–9988.
(11) Hong, D. Y.; Hwang, Y. K.; Serre, C.; Ferey, G.; Chang, J. S. *Adv. Funct. Mater.* **2009**, *19*, 1537–1552.
(12) Das, S.; Kim, H.; Kim, K. *J. Am. Chem. Soc.* **2009**, *131*, 3814–3815.
(13) Gascon, J.; Aktay, U.; Hernandez-Alonso, M. D.; van Klink, G. P. M.; Kapteijn, F. *J. Catal.* **2009**, *261*, 75–87.
(14) Jiang, D. M.; Urakawa, A.; Yulikov, M.; Mallat, T.; Jeschke, G.; Baiker, A. *Chem.—Eur. J.* **2009**, *15*, 12255–12262.
(15) Natarajan, S.; Mahata, P. *Chem. Soc. Rev.* **2009**, *38*, 2304–2318.
(16) Lee, J.; Farha, O. K.; Roberts, J.; Scheidt, K. A.; Nguyen, S. T.; Hupp, J. T. *Chem. Soc. Rev.* **2009**, *38*, 1450–1459.
(17) (a) Shultz, A. M.; Farha, O. K.; Hupp, J. T.; Nguyen, S. T. *J. Am. Chem. Soc.* **2009**, *131*, 4204–4205. (b) Nelson, A. P.; Farha, O. K.; Mulfort, K. L.; Hupp, J. T. *J. Am. Chem. Soc.* **2009**, *131*, 458–460.
(18) Lu, Y.; Tonigold, M.; Bredenkotter, B.; Volkmer, D.; Hitzbleck, J.; Langstein, G. *Z. Anorg. Allg. Chem.* **2008**, *634*, 2411–2417.
(19) Proch, S.; Herrmannsdorfer, J.; Kempe, R.; Kern, C.; Jess, A.; Seyfarth, L.; Senker, J. *Chem.—Eur. J.* **2008**, *14*, 8204–8212.
(20) Ingleson, M. J.; Barrio, J. P.; Guilbaud, J. B.; Khimyak, Y. Z.; Rosseinsky, M. J. *Chem. Commun.* **2008**, 2680–2682.
(21) Wu, C. D.; Hu, A.; Zhang, L.; Lin, W. B. *J. Am. Chem. Soc.* **2005**, *127*, 8940–8941.
(22) Corma, A.; Garcia, H.; Llabrs i Xamena, F. X. *Chem. Rev.* **2010**, DOI: 10.1021/cr9003924.

Published on Web 07/21/2010

Scheme 1. Schematic Representation of the Thermal Decomposition of $Cr(CO)_6$ in the Presence of an Arene Moiety, with Consequent Formation of (η^6-arene)$Cr(CO)_3$ Species, Followed by the Release of CO

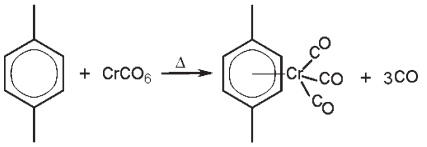

Indeed, there exist several examples of organometallic species where the metal site is coordinated to a π-donor arene ring. This strategy has been followed recently by Kaye and Long,[23] who successfully functionalized MOF-5 by grafting $Cr(CO)_3$ units on the benzene ring of the organic linker; and by Kamegawa et al.,[24] who reported the functionalization of an inorganic−organic hybrid mesoporous silica with the same species. In both cases, the functionalization proceeded through thermal decomposition of $Cr(CO)_6$ precursor, following the reaction reported in Scheme 1.

The (η^6-arene)$Cr(CO)_3$ species are particularly interesting, because they play important roles in heterogeneous catalysis (e.g., hydrogenation of polyunsaturates into cis-unsaturated products) and are building blocks in organometallic chemistry.[25,26] Moreover, $M(CO)_n$ units have been found to substitute at least one CO ligand with one N_2 or H_2 under irradiation with ultraviolet (UV) light (following the reaction shown in Scheme 2),[27−31] which is a behavior that opens interesting perspectives in the field of the storage of small molecules.

As a consequence of these first (rapid) communications, many efforts have been devoted to the theoretical estimation of the stability and reactivity of $Cr(CO)_3$ species grafted on benzene rings, as a function of the electron-donor or electron-acceptor nature of the ring substituent.[32−35] Very recently, some of us have demonstrated that a relationship exists between the stability of the grafted (η^6-arene)$Cr(CO)_3$ adducts and experimentally valuable quantities, as obtained by X-ray diffraction

Scheme 2. Schematic Representation of the UV-Induced CO Substitution by N_2 Ligand for (η^6-arene)$Cr(CO)_3$ Species, with an Attendant Release of CO

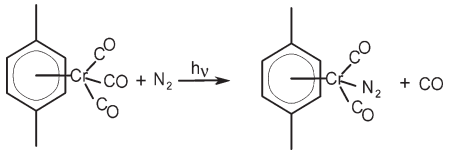

(XRD), X-ray absorption spectroscopy (XAS), and Fourier transform infrared (FT-IR) spectroscopy.[36]

In the present work, we report on the functionalization of the recently synthesized UiO-66 material with $Cr(CO)_3$ moieties. UiO-66 is a cubic close-packed three-dimensional metal−organic framework composed by a zirconia-based inorganic building brick and 1,4-benzene dicarboxylic acid (H_2BDC) as organic linker;[37] the Zr sites do not present any coordination vacancy. For this reason, the obtained results can be directly compared with those obtained by functionalizing a completely organic material, i.e., a poly(styrene-co-divinylbenzene) resin (hereafter referenced as PS). Despite its amorphous nature, the PS matrix presents a very high surface area and a porosity very similar to those displayed by the UiO-66 material, which are achieved through a high cross-linking degree. Therefore, it offers a good opportunity to evaluate experimentally the influence of the ring substituent on the structural, electronic, and vibrational properties of the grafted $Cr(CO)_3$. The formation, reversibility and stability of the two systems are systematically investigated by FT-IR, ultraviolet−visible (UV−vis), X-ray absorption near-edge structure (XANES), and extended X-ray absorption fine structure (EXAFS) spectroscopies, complemented by quantum mechanical calculations. Moreover, the photoinduced reactivity of $Cr(CO)_3$ in UiO-66 is also explored, by following the substitution of one CO ligand with a N_2 molecule. Finally, complementary results obtained in the case of the similar $Mo(CO)_3$ grafted species are reported in the Supporting Information, for the purpose of showing the role of the metal in affecting the investigated properties.

Although the possibility to functionalize hybrid organic/inorganic structures by means of $M(CO)_n$ species has been already reported in the past,[23,24] the occurrence of a similar reactivity in the case of completely organic matrices (such as PS) has never been shown. Moreover, a complete vibrational, electronic, and (especially) structural characterization by means of several spectroscopic techniques coupled with theoretical calculations is still missing. The present work (i) has the ambitious goal to completely describe the functionalization of two categories of porous materials (metal−organic frameworks and cross-linked polymers) by means of an organometallic approach, and (ii) would like to become the starting point for the development of a systematic procedure of investigation of functionalized porous matrices.

(23) Kaye, S. S.; Long, J. R. *J. Am. Chem. Soc.* **2008**, *130*, 806–807.
(24) Kamegawa, T.; Sakai, T.; Matsuoka, M.; Anpo, M. *J. Am. Chem. Soc.* **2005**, *127*, 16784–16785.
(25) Rosillo, M.; Dominguez, G.; Perez-Castells, J. *Chem. Soc. Rev.* **2007**, *36*, 1589–1604.
(26) Gibson, S. E.; Ibrahim, H. *Chem. Commun.* **2002**, 2465–2473.
(27) Upmacis, R. K.; Poliakoff, M.; Turner, J. J. *J. Am. Chem. Soc.* **1986**, *108*, 3645–3651.
(28) Sweany, R. L. *J. Am. Chem. Soc.* **1985**, *107*, 2374–2379.
(29) Howdle, S. M.; Healy, M. A.; Poliakoff, M. *J. Am. Chem. Soc.* **1990**, *112*, 4804–4813.
(30) Goff, S. E. J.; Nolan, T. F.; George, M. W.; Poliakoff, M. *Organometallics* **1998**, *17*, 2730–2737.
(31) Zheng, Y.; Wang, W.; Lin, J.; She, Y.; Fu, K. *J. Phys. Chem.* **1992**, *96*, 9821–9827.
(32) Suresh, C. H.; Koga, N.; Gadre, S. R. *Organometallics* **2000**, *19*, 3008–3015.
(33) Lochan, R. C.; Khaliullin, R. Z.; Head-Gordon, M. *Inorg. Chem.* **2008**, *47*, 4032–4044.
(34) Alamiry, M. A. H.; Brennan, P.; Long, C.; Pryce, M. T. *J. Organomet. Chem.* **2008**, *693*, 2907–2914.
(35) Alamiry, M. A. H.; Boyle, N. M.; Brookes, C. M.; George, M. W.; Long, C.; Portius, P.; Pryce, M. T.; Ronayne, K. L.; Sun, X. Z.; Towrie, M.; Vuong, K. Q. *Organometallics* **2009**, *28*, 1461–1468.
(36) Vitillo, J. G.; Groppo, E.; Bordiga, S.; Chavan, S.; Ricchiardi, G.; Zecchina, A. *Inorg. Chem.* **2009**, *48*, 5439–5448.
(37) Cavka, J. H.; Jakobsen, S.; Olsbye, U.; Guillou, N.; Lamberti, C.; Bordiga, S.; Lillerud, K. P. *J. Am. Chem. Soc.* **2008**, *130*, 13850–13851.

2. Materials and Methods

2.1. Materials. *UiO-66*. UiO-66 is a cubic close-packed three-dimensional (3D) metal−organic framework comprised of a zirconia-based inorganic building brick ($Zr_6O_4(OH)_4(CO_2)_{12}$) and 1,4-benzene dicarboxylic acid (H_2BDC) as a organic linker. The details of the structure and synthesis have been reported elsewhere.[37] In the typical synthesis, a mixture of $ZrCl_4$ and H_2BDC in *N*,*N*′-dimethyl formamide is heated in a sealed container at 120 °C for 24 h. The material, stable up to 375 °C, crystallized as small (0.2 μm) intergrown cubic crystals. UiO-66 has a Langmuir surface area of 1187 $m^2\,g^{-1}$ (BET = 1080 $m^2\,g^{-1}$) and pores with openings ranging from 6 Å to 10 Å.

PS. The cross-linked polymer used in these experiments is a poly(styrene-co-divinylbenzene) resin commercialized by Aldrich in the form of 300−800 μm beads. The polymer presents a BET surface area of 1000 $m^2\,g^{-1}$, as evaluated by N_2 adsorption measurement at 77 K, and a pore size distribution centered at ~16 Å.[38] The permanent open texture characterizing this porous polymeric matrix is obtained by 25% cross-linking level with divinylbenzene, and allows the easy diffusion of molecules from the gas phase.

$Cr(CO)_6$ and (η^6-C_6H_6)$Cr(CO)_3$ were obtained from Strem Chemicals Co. and Aldrich, respectively, and used without any treatment.

In Situ Formation of the (arene)M(CO)$_3$ Species. Prior to the dosage of metal hexacarbonyls, both UiO-66 and PS have been activated under vacuum to remove all the adsorbates (solvents and water), each one at the proper experimental conditions, i.e., at 250 °C (for 30 min) and at room temperature (for 60 min), respectively. $M(CO)_6$ (M = Cr or Mo) was then dosed from the gas phase upon vacuum sublimation of the solid at room temperature. Finally, the matrices were treated in the presence of $M(CO)_6$ at 150 °C (i.e., below the decomposition temperature of $Cr(CO)_6$), to optimize the formation of the (arene)$M(CO)_3$ species (see section 3.1). The stability of both the $M(CO)_6$ precursor and the $M(CO)_3$ products is different in the two matrices, as will be discussed in the following. As far as functionalized PS is concerned, an X-ray absorption spectrum (vide infra section 2.2.1) has been collected in transmission mode to evaluate the Cr loading, resulting in an approximate loading of 1 wt %. The same order of magnitude of Cr loading has been obtained for the functionalized UiO-66, as both samples resulted in IR spectra of comparable intensity in the C−O stretching region. Accessibility of pores after functionalization has been proved by in situ IR experiments, showing that N_2, under UV irradiation, is able to substitute a CO ligand, according to Scheme 2 (vide infra section 3.2).

2.2. Methods. *2.2.1. Experimental Section*. FTIR spectra were collected in transmission mode at a resolution of 2 cm^{-1} on a Bruker IFS66 spectrophotometer equipped with both MCT and DTGS detectors. The experiments have been performed either on self-supporting pellets and thin depositions on silicon, as described previously.[39] For $Cr(CO)_6$ and (C_6H_6)$Cr(CO)_3$ in THF solution, the IR measurements were performed in a cell for liquids. Parallel DR−UV−vis−NIR measurements were performed on a Varian Cary 5000 spectrometer equipped with a reflectance sphere on thick self-supported pellets. In all experiments, samples were put inside ad hoc cells that allow thermal treatments under high vacuum conditions, dosage of probe molecules, and in situ spectra collection to be performed.

X-ray absorption experiments at the Cr K-edge (5989 eV) were performed at the BM26A beamline (DUBBLE) of the ESRF facility (Grenoble, France).[40] The white beam was monochromatized using a Si(111) double crystal; harmonic rejection has been performed using a meridionally focusing mirror with an angle of incidence of 2.8 mrad and a silicon coating. The spectra of the (η^6-C_6H_6)-$Cr(CO)_3$ and $Cr(CO)_6$ reference samples have been collected in transmission mode, on self-supporting pellets diluted with boron nitride (BN). In contrast, for PS/$Cr(CO)_3$ EXAFS spectra were collected in fluorescence mode because of the chromium dilution, by means of a nine-element Ge monolithic detector. To avoid contamination, the sample was sealed in a glass capillary (1.5 mm in diameter), following the well-established procedure adopted for powder XRD (XRPD) experiments.[41] For this reason, the beam was vertically focused to reach a dimension of 0.3 mm on the sample. The horizontal slits were optimized to fit with the interval of uniform filling of the capillary. This procedure, which is common in XRPD measurements, is not standard for EXAFS measurements, because it requires a very stable beam along the entire energy scan. We have successfully applied this strategy in previous cases.[42,43]

The XANES part of the spectra was acquired with an energy step of 0.4 eV and an integration time of 2 s/point. The EXAFS part of the spectra was collected up to 12 $Å^{-1}$ with a variable sampling step in energy, resulting in Δk = 0.05 $Å^{-1}$, and an integration time that linearly increases as a function of k from 5 s/point to 20 s/point to account for the low signal-to-noise ratio at high k-values. For each sample, three equivalent EXAFS spectra were acquired and averaged before the data analysis.[44] EXAFS data

(38) Spoto, G.; Vitillo, J. G.; Cocina, D.; Damin, A.; Bonino, F.; Zecchina, A. *Phys. Chem. Chem. Phys.* **2007**, *9*, 4992–4999.

(39) Chavan, S.; Bonino, F.; Vitillo, J. G.; Groppo, E.; Lamberti, C.; Dietzel, P. D. C.; Zecchina, A.; Bordiga, S. *Phys. Chem. Chem. Phys.* **2009**, *11*, 9811–9822.

(40) Nikitenko, S.; Beale, A. M.; van der Eerden, A. M. J.; Jacques, S. D. M.; Leynaud, O.; O'Brien, M. G.; Detollenaere, D.; Kaptein, R.; Weckhuysen, B. M.; Bras, W. *J. Synchrot. Radiat.* **2008**, *15*, 632–640.

(41) Palomino, G. T.; Bordiga, S.; Zecchina, A.; Marra, G. L.; Lamberti, C. *J. Phys. Chem. B* **2000**, *104*, 8641–8651.

(42) Estephane, J.; Groppo, E.; Damin, A.; Vitillo, J. G.; Gianolio, D.; Lamberti, C.; Bordiga, S.; Prestipino, C.; Nikitenko, S.; Quadrelli, E. A.; Taoufik, M.; Basset, J. M.; Zecchina, A. *J. Phys. Chem. C* **2009**, *113*, 7305–7315.

(43) Gianolio, D.; Groppo, E.; Vitillo, J. G.; Damin, A.; Bordiga, S.; Zecchina, A.; Lamberti, C. *Chem. Commun.* **2010**, *46*, 976–978.

(44) Lamberti, C.; Bordiga, S.; Arduino, D.; Zecchina, A.; Geobaldo, F.; Spanò, G.; Genoni, F.; Petrini, G.; Carati, A.; Villain, F.; Vlaic, G. J. *J. Phys. Chem. B* **1998**, *102*, 6382–6390.

analysis was performed using the Arthemis software,[45] following the strategy reported in details in the Supporting Information.

2.2.2. Theoretical Calculations. The calculations have been performed with the Gaussian 03 software package[46] at the B3LYP level of calculation.[47,48] The PS and UiO-66 frameworks have been modeled by means of benzene and p-$C_6H_4(COOH)_2$, respectively. These cluster models have been successfully used to reproduce the CO vibrational shifts of grafted $Cr(CO)_3$ species on MOFs in ref 36. For the H atoms, the standard Pople basis set supplemented by diffuse and polarizability functions 6-311++G(2d,2p) has been adopted.[49,50] For all the other elements, the fully optimized triple-ζ valence basis sets proposed by Ahlrichs et al.[51] have been used, augmented by two sets of polarization functions derived from the original ones, following an even-tempered recipe that is by substituting the polarization orbital in the basis set with two orbitals, having, respectively, the coefficient doubled and halved with respect to the parent orbital. The so-obtained basis sets will be indicated as TZV2p. Geometry optimization has been carried out by means of the Berny optimization algorithm with an analytical gradient. No geometrical constraints have been imposed. For further details on the calculations, please refer to ref 36.

Harmonic frequencies have been obtained by determining the second derivatives of the energy analytically, with respect to the Cartesian nuclear coordinates, and then transforming to mass-weighted coordinates. No scaling factor has been adopted.

The UV−vis spectra were obtained from time-dependent density functional theory (TDDFT)[52,53] calculations for the (η^6-C_6H_6)$Cr(CO)_3$ and [η^6-$C_6H_4(COOH)_2$]$Cr(CO)_3$ complexes in the gas phase. TDDFT is well-known as a rigorous formalism for the treatment of excitation energies within the DFT. In particular, it has been successfully applied in the literature for the calculation of excitation energies of metal complexes.[34,54−56] A total of 100 singlet excited states and their corresponding oscillator strengths were determined. The theoretical spectrum was obtained through a Gaussian convolution of the peaks using the Gauss View 4.1 Program. The electronic distribution and localization of the singlet excited states were visualized using electron density difference maps.

3. Results and Discussion

3.1. Formation and Stability of (arene)$Cr(CO)_3$ Complexes. *3.1.1. Vibrational Properties: In Situ FT-IR Spectroscopy*. $Cr(CO)_6$ in the gas phase is characterized by four IR-active modes of T_{1u} symmetry:[57] CO stretching, ν(CO); metal−carbon−oxygen bending, δ(Cr−C−O); metal−carbon stretching, ν(Cr−C); and carbon−metal−carbon deformation, def(C−Cr−C); these modes give rise to four IR absorption bands, centered at 2000, 668, 440, and 98 cm^{-1}, respectively. Because of instrumental limitations, only the ν(CO) and δ(Cr−C−O) regions were accessible and, therefore, only these two regions will be discussed in the following. When $Cr(CO)_6$ is dissolved in THF (dark gray curve in Figure 1b), its molecular symmetry is slightly perturbed. As a consequence, the IR absorption bands slightly shift in frequency (ν(CO) at 1979 cm^{-1} and δ(Cr−C−O) at 665 cm^{-1}) and also the Raman-active ν(CO) vibration of E_g symmetry becomes visible (weak band at 2020 cm^{-1}). A similar "solvent effect" is also observed when $Cr(CO)_6$ is adsorbed inside both PS and UiO-66 matrices (dark gray curves in Figures 1c and 1d): the IR spectra are dominated by a very intense, out-of-scale, IR absorption band centered at ∼1980 cm^{-1} (IR-active mode) and by a weaker band at ∼2020 cm^{-1} (Raman active).[58] Similar bands have been reported previously in the case of $Cr(CO)_6$ adsorbed on oxides.[59−61] In the low-frequency range, the band associated with δ(Cr−C−O) is observed at ∼664 cm^{-1} in both cases.

Even though the vibrational features of $Cr(CO)_6$ physisorbed in PS and UiO-66 are very similar, the two systems show strong differences in their stability upon evacuation. In particular, in the case of PS, the adsorbed $Cr(CO)_6$ is completely removed by outgassing at room temperature, whereas, in the case of UiO-66, $Cr(CO)_6$ is almost irreversibly adsorbed at room temperature, and it can be removed only upon prolonged outgassing at 150 °C. This is in agreement with what is expected on an

(45) Ravel, B.; Newville, M. *Phys. Scr.* **2005**, *T115*, 1007–1010.
(46) Frisch, M. J.; Trucks, G. W.; Schlegel, H. B.; Scuseria, G. E.; Robb, M. A.; Cheeseman, J. R.; Montgomery, J., J. A.; Vreven, T.; Kudin, K. N.; Burant, J. C.; Millam, J. M.; Iyengar, S. S.; Tomasi, J.; Barone, V.; Mennucci, B.; Cossi, M.; Scalmani, G.; Rega, N.; Petersson, G. A.; Nakatsuji, H.; Hada, M.; Ehara, M.; Toyota, K.; Fukuda, R.; Hasegawa, J.; Ishida, M.; Nakajima, T.; Honda, Y.; Kitao, O.; Nakai, H.; Klene, M.; Li, X.; Knox, J. E.; Hratchian, H. P.; Cross, J. B.; Bakken, V.; Adamo, C.; Jaramillo, J.; Gomperts, R.; Stratmann, R. E.; Yazyev, O.; Austin, A. J.; Cammi, R.; Pomelli, C.; Ochterski, J. W.; Ayala, P. Y.; Morokuma, K.; Voth, G. A.; Salvador, P.; Dannenberg, J. J.; Zakrzewski, V. G.; Dapprich, S.; Daniels, A. D.; Strain, M. C.; Farkas, O.; Malick, D. K.; Rabuck, A. D.; Raghavachari, K.; Foresman, J. B.; Ortiz, J. V.; Cui, Q.; Baboul, A. G.; Clifford, S.; Cioslowski, J.; Stefanov, B. B.; Liu, G.; Liashenko, A.; Piskorz, P.; Komaromi, I.; Martin, R. L.; Fox, D. J.; Keith, T.; Al-Laham, M. A.; Peng, C. Y.; Nanayakkara, A.; Challacombe, M.; Gill, P. M. W.; Johnson, B.; Chen, W.; Wong, M. W.; Gonzalez, C.; Pople, J. A. Gaussian 2004, Revision B.05, Wallingford, CT, 2004.
(47) Becke, A. D. *J. Chem. Phys.* **1993**, *98*, 5648–5652.
(48) Lee, C.; Yang, W.; Parr, R. G. *Phys. Rev. B* **1988**, *37*, 785–789.
(49) Clark, T.; Chandrasekhar, J.; Spitznagel, G. W.; Schleyer, P. v. R. *J. Comput. Chem.* **1983**, *4*, 294–301.
(50) Frisch, M. J.; Pople, J. A.; Binkley, J. S. *J. Chem. Phys.* **1984**, *80*, 3265–3269.
(51) Schäfer, A.; Huber, C.; Ahlrichs, R. *J. Chem. Phys.* **1994**, *100*, 5829–5835.
(52) Casida, M. E.; Jamorski, C.; Casida, K. C.; Salahub, D. R. *J. Chem. Phys.* **1998**, *108*, 4439–4449.
(53) Stratmann, R. E.; Scuseria, G. E.; Frisch, M. J. *J. Chem. Phys.* **1998**, *109*, 8218–8224.
(54) Ciofini, I.; Laine, P. P.; Bedioui, F.; Adamo, C. *J. Am. Chem. Soc.* **2004**, *126*, 10763–10777.
(55) Salassa, L.; Garino, C.; Salassa, G.; Gobetto, R.; Nervi, C. *J. Am. Chem. Soc.* **2008**, *130*, 9590–9597.
(56) Vlček, A. *Coord. Chem. Rev.* **1998**, *177*, 219–256.
(57) Adams, D. M., *Metal−Ligand and Related Vibrations*; Edward Arnold (Publisher) Ltd.: London, 1967.
(58) The very weak, Raman-active, ν_1 mode also is slightly visible ∼2110 cm^{-1}.
(59) Guglielminotti, E. *J. Mol. Catal.* **1981**, *13*, 207–214.
(60) Platero, E. E.; Arean, C. O.; Scarano, D.; Spoto, G.; Zecchina, A. *Mater. Chem. Phys.* **1991**, *29*, 347–355.
(61) Zecchina, A.; Arean, C. O. *Catal. Rev.−Sci. Eng.* **1993**, *35*, 261–317.

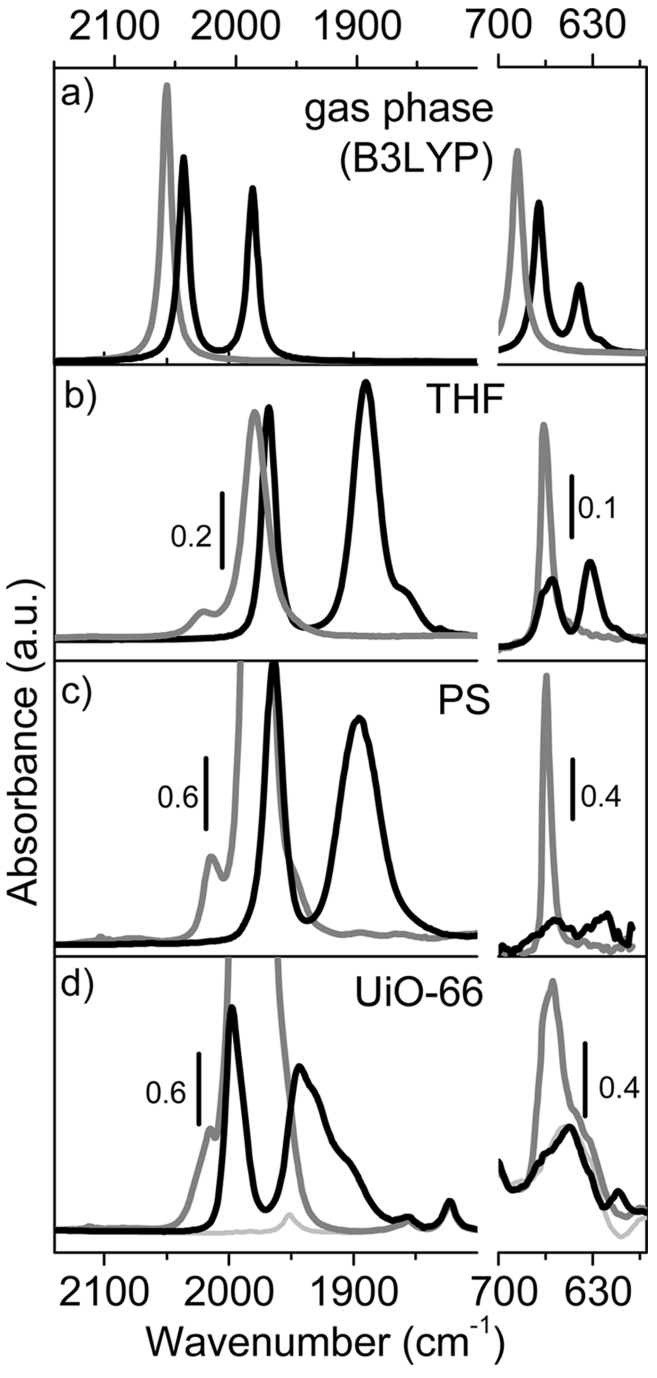

Figure 1. FTIR spectra of $Cr(CO)_6$ (dark gray trace) and (η^6-C_6H_6)Cr-$(CO)_3$ (black trace) as (a) obtained by B3LYP calculation (unscaled spectra), and experimentally determined in (b) THF, (c) PS, and (d) UiO-66 supports. The left and right portions of each panel display the ν(CO) and δ(Cr−C−O) regions, respectively. In panels (b) and (c), background subtracted spectra are reported, whereas in panel (d), the spectrum of the UiO-66 is reported as the light gray trace.

electrostatic basis.[36] Because of this difference, the grafting of $Cr(CO)_3$ via thermal decomposition of $Cr(CO)_6$ was performed following two different procedures: (i) by heating at 150 °C for 12 h in closed cell, followed by outgassing at room temperature, in the case of PS; (ii) by heating at 150 °C for 12 h under dynamic vacuum, in the case of UiO-66. After the thermal treatment, both samples become colored (light and dark yellow, respectively, vide infra the UV−vis spectra in section 3.1.2), suggesting the formation of (arene)$Cr(CO)_3$ species. Indeed, the FT-IR spectra obtained after the thermal decomposition of $Cr(CO)_6$ are dominated by two new IR absorption bands in the ν(CO) region (black curves in Figure 1c and 1d), at a lower frequency, with respect to the $Cr(CO)_6$ bands. These two bands, which are very similar to those observed in the case of (η^6-C_6H_6)$Cr(CO)_3$ in THF (black curve in Figure 1b), are easily assigned to the nondegenerate total symmetric stretching $\nu(CO_{totsym})$ and to the doubly degenerate total asymmetric stretching $\nu(CO_{asym})$ of the (arene)$Cr(CO)_3$ species.[57] A qualitative picture of the bonding in transition-metal π-complexes involves a donation of charge from the arene to the metal and then, in turn, from the metal to the carbonyl groups, which results into an increase of the strength of the Cr−CO bond, compared to $Cr(CO)_6$, and into a decrease of the C−O bond strength, compared to $Cr(CO)_6$ and CO.[36,62] This explains why the vibrational modes of the (arene)$Cr(CO)_3$ species are at lower frequency, with respect to those of $Cr(CO)_6$. In the low-frequency range, the disappearance of the sharp band at ~664 cm^{-1} confirms the absence of unreacted $Cr(CO)_6$, while the attendant appearance of weak bands in the δ(Cr−C−O) region, at 659 and 620 cm^{-1} for PS/$Cr(CO)_3$ and at 610 cm^{-1} for UiO-66/$Cr(CO)_3$, is associated with the formation of (arene)$Cr(CO)_3$ species (compare the same region for (η^6-C_6H_6)$Cr(CO)_3$ in THF, Figure 1b). Note that the changes observed in the experimental spectra before and after the thermal treatment correspond to the difference in the computed spectra of $Cr(CO)_6$ and (η^6-C_6H_6)$Cr(CO)_3$, respectively (unscaled, Figure 1a).

Entering in more details, the PS/$Cr(CO)_3$ system (black spectrum in Figure 1c) shows a narrow IR absorption band at 1966 cm^{-1} and a broader one at 1898 cm^{-1}, very close to those of (η^6-C_6H_6)$Cr(CO)_3$ in THF (black curve in Figure 1b), whereas the same bands appear at 1998 and 1944 cm^{-1}, respectively, in the case of the UiO-66/$Cr(CO)_3$ system (black curve in Figure 1d). The blue-shift of the ν(CO) bands in the case of UiO-66/$Cr(CO)_3$ can be explained by considering the electron-accepting nature of the arene substituent, as recently demonstrated by Vitillo et al.[36] Basically, an electron-accepting substituent on the ring (such as the carboxylate of the UiO-66 matrix) decreases the charge transfer to the metal and further decreases the Cr−CO bond order, while, at the same time, increases the C−O bond order, compared to the unsubstituted complex.

Beside the different frequency position, the two IR absorption bands characterizing PS/$Cr(CO)_3$ and UiO-66/$Cr(CO)_3$ have a larger full-width at half-maximum (fwhm), with respect to the pure (η^6-C_6H_6)$Cr(CO)_3$, although the relative ratio of the fwhm values of the two bands is the same. This evidence suggests a higher heterogeneity of the grafted species in the two investigated supports. Moreover, in the case of the UiO-66/$Cr(CO)_3$ system, the band centered at 1944 cm^{-1} is constituted by at least three different components (at 1943, 1929, and 1904 cm^{-1}), a

(62) Carrol, D. G.; McGlykn, S. P. *Inorg. Chem.* **1968**, *7*, 1285–1290.

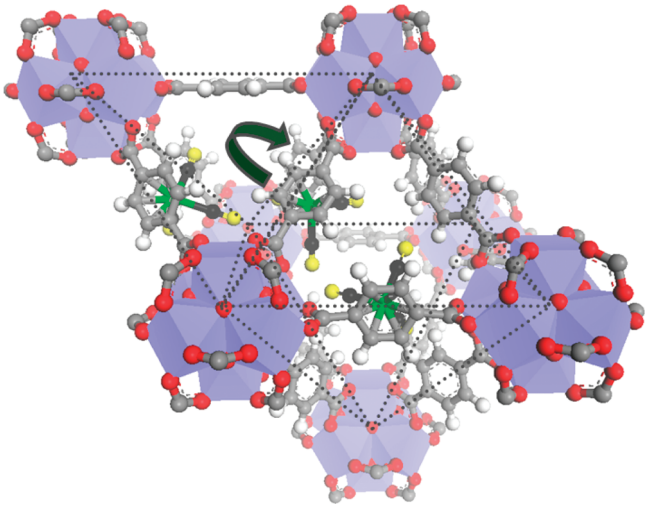

Figure 2. Graphic representation of (arene)$Cr(CO)_3$ species formed inside UiO-66; the tetrahedral and hexahedral cages are emphasized by dotted gray lines. The Zr atoms are represented as blue octahedra with O (red) at the corners; C and H atoms are shown in gray and white, respectively. Cr, C, and O of the $Cr(CO)_3$ moieties are reported in green, dark gray, and yellow, respectively. The green arrow illustrates that a rotation by 45° of the benzene ring will move the $Cr(CO)_3$ from one cage to the neighboring cage.

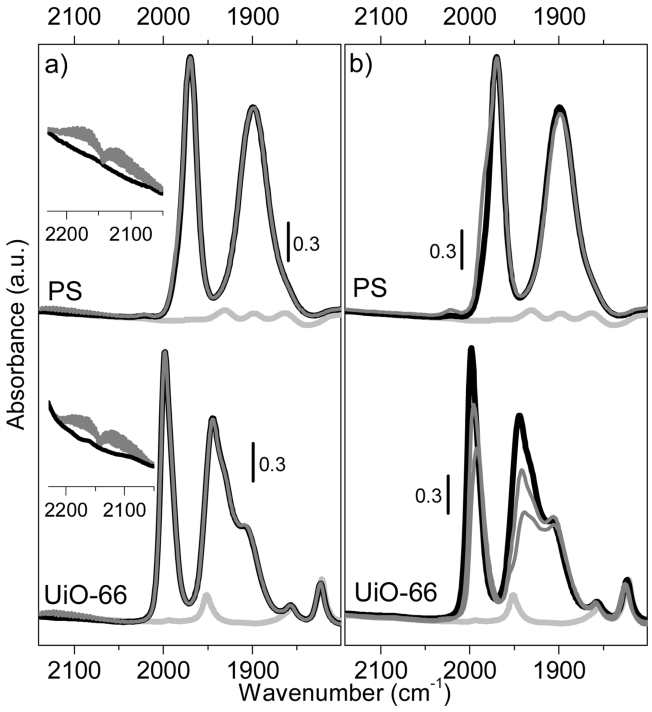

Figure 3. (a) Reversibility in the presence of CO and (b) stability in air of the (arene)$Cr(CO)_3$ species formed in PS (top) and in UiO-66 (bottom). Light gray, spectrum of the matrix before $Cr(CO)_6$ dosage; black, (arene)-$Cr(CO)_3$; dark gray, evolution upon CO dosage or exposure to air. Insets in panel a show a magnification of the 2250−2030 cm^{-1}, where the roto-vibrational profile of gaseous CO is present.

fact that can be explained by considering the fact that the $Cr(CO)_3$ moieties feel slightly different environments. Indeed, the local environment of a $Cr(CO)_3$ species in UiO-66 is quite complex. UiO-66 is characterized by two type of cages: a tetrahedral one (smaller) and a hexahedral one (larger), each accounting for half of the volume and each with the same entrance windows, as reported in

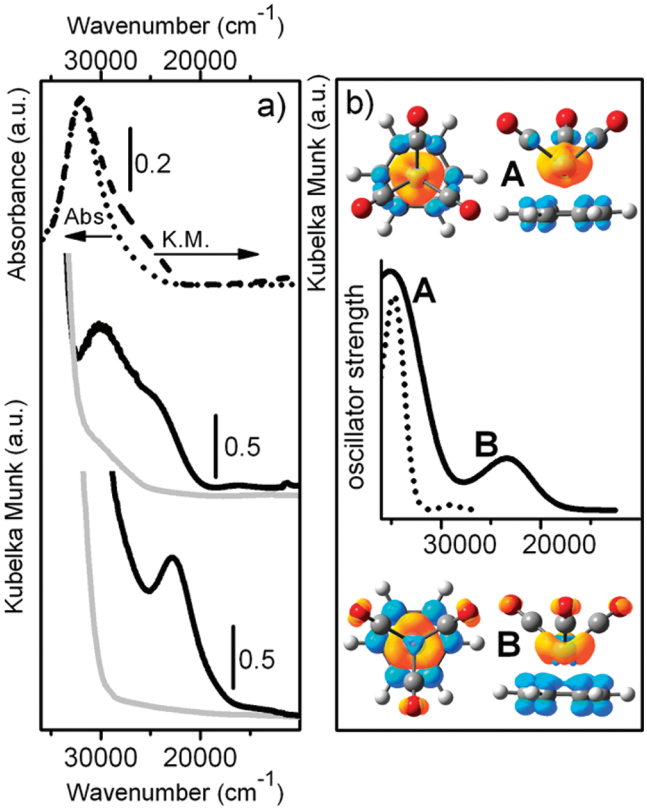

Figure 4. (a) Experimental UV−vis spectra of the (arene)$Cr(CO)_3$ species. The top part shows data for the bare (η^6-C_6H_6)$Cr(CO)_3$ sample in the solid state (diluted in silica, in DR mode; represented by the dashed curve) and in ethanol solution (in transmission mode; represented by the dotted curve), whereas the middle and bottom parts show data for (arene)$Cr(CO)_3$ formed inside PS and in UiO-66 samples, respectively (black curves). Gray curves refer to the spectra of the corresponding empty supports. (b) TDDFT optical spectra of (C_6H_6)$Cr(CO)_3$ and (p-C_6H_4)$(COOH)_2Cr(CO)_3$ (dotted and full lines, respectively), where the top and bottom parts display the difference in the electron density of the states involved in the A and B electronic transitions (blue, positive values; orange, negative values).

Figure 2 (dotted gray lines). Because of the steric encumbrance, only one $Cr(CO)_3$ species can be hosted in the tetrahedral cage, whereas two functionalities can found place in the hexahedral one, provided that they are formed on two opposite benzene rings. From the graphical representation reported in Figure 2, it is clear that the carbonyl species are surrounded by a different environment in the two type of cages; this is likely the origin of the slightly different vibrational properties highlighted by FT-IR spectroscopy. Finally, note that the structure of UiO-66 is completely retained after the functionalization, as demonstrated by XRPD data (collected in a controlled atmosphere; see Figure S1 in the Supporting Information).

The as-formed (arene)$Cr(CO)_3$ species are stable in the presence of CO (at least for a few hours), i.e., they are not converted back to $Cr(CO)_6$. This is evident in Figure 3a, as no changes in the FT-IR spectra of the (arene)$Cr(CO)_3$ complexes are observed when 40 mbar of CO are dosed at room temperature. On the contrary, the formed complexes are less stable in the presence of air/moisture (see Figure 3b). The stability is greater when the complexes are formed in a hydrophobic matrix (PS) with respect to the

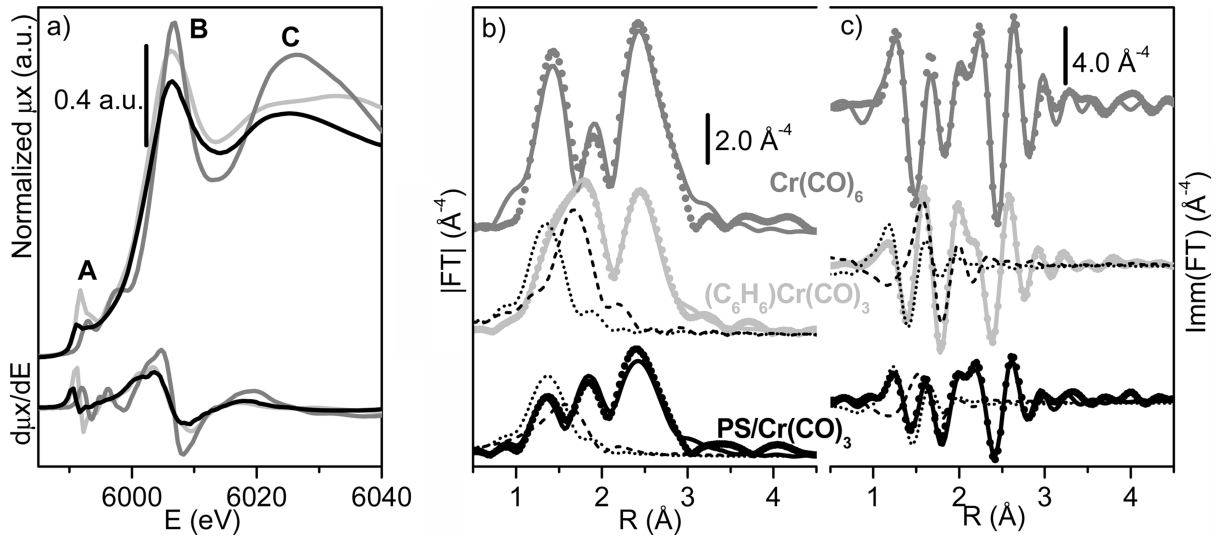

Figure 5. (a) XANES spectra of PS/$Cr(CO)_3$ species (black trace), compared to those of the (η^6-C_6H_6)$Cr(CO)_3$ (light gray trace) and $Cr(CO)_6$ (gray trace) reference compounds. Both the normalized μx and the derivative spectra are reported (top and bottom parts, respectively). (b and c) The k^3-weighted, phase-uncorrected, Fourier transform (FT) of the EXAFS spectra of PS/$Cr(CO)_3$ species (bottom), compared to those of the (η^6-C_6H_6)$Cr(CO)_3$ (middle) and $Cr(CO)_6$ (top) reference compounds. in modulus and imaginary parts, respectively. The experimental data (scattered circles) are compared with the best fits (full line). In the case of PS/$Cr(CO)_3$ and (η^6-C_6H_6)$Cr(CO)_3$, dotted and dashed curves are the first shell SS contributions due to $Cr-C_{CO}$ and $Cr-C_{Bz}$, respectively, as estimated by the best fit.

more hydrophilic one (UiO-66). The stability of the corresponding (arene)$Mo(CO)_3$ complexes in UiO-66 and PS also has been characterized, and the results are reported in the Supporting Information. As a general statement, the stability of (arene)$M(CO)_3$, both in the presence of CO and of air/moisture, follows the order Cr > Mo. A considerable formation of $Mo(CO)_6$ species in the presence of CO is observed, whereas, upon exposure to moisture, the complexes are almost completely decomposed (see Figure S3 in the Supporting Information).

3.1.2. Optical Properties: In Situ DR UV−vis−NIR Spectroscopy. As already anticipated in the previous section, upon heating the PS and UiO-66 matrices in the presence of $Cr(CO)_6$, the samples became colored, pale, and dark yellow in the two cases, respectively, in close analogy to the bright yellow color of the (η^6-C_6H_6)$Cr(CO)_3$ reference compound. The UV−vis spectrum of (η^6-C_6H_6)$Cr(CO)_3$ in ethanol solution (dotted curve in the top part of Figure 4a) shows a well-defined band centered at ~32 000 cm^{-1}. The spectrum of solid (η^6-C_6H_6)$Cr(CO)_3$ (diluted in silica; represented by the dashed curve in the top part of Figure 4a) also displays a shoulder at ~26 500 cm^{-1}. Theoretical calculations assign these absorption bands to a charge transfer from the $Cr(CO)_3$ fragment to the benzene ring, in agreement with the literature.[34,62] The simulated optical spectrum for (η^6-C_6H_6)$Cr(CO)_3$ in the gas phase is displayed in Figure 4b (dotted curve), together with a graphical representation of the corresponding electronic transitions (electron density moves from orange orbitals to the blue ones). Note that two transitions are predicted at ~35 000 (band A) and 29 000 cm^{-1} (band B), and the second one is almost forbidden. Transitions implying an electron density movement from the (η^6-C_6H_6)Cr moiety to the carbonyl ligands occur at higher frequencies and are not considered in this work.

Similar bands in the visible region are observed in the case of the (arene)$Cr(CO)_3$ species formed inside PS and UiO-66 matrices, as reported in central and bottom parts of Figure 4a (full black curves). In both cases, the intense absorption band with an edge at ~30 000 cm^{-1} is assigned to the $\pi-\pi^*$ transition of the arene moieties characterizing the matrices (compare the spectra with those of the corresponding pure matrices, gray curves). Besides this feature, the spectrum of the PS/$Cr(CO)_3$ system shows a complex band centered at ~28 000 cm^{-1}, with two components at 30 000 and 25 000 cm^{-1}. For UiO-66/$Cr(CO)_3$, the optical spectrum displays an intense, out-of-scale, band at ~30000 cm^{-1} and a well-defined one at 23 000 cm^{-1}. In close analogy with (η^6-C_6H_6)$Cr(CO)_3$, these absorption bands are associated with $(CO)_3Cr \rightarrow$ arene charge-transfer transitions. We expect that the different electron-donor nature of the arene substituent should affect the frequency position of the two components. By comparing the results of calculations performed on (C_6H_4)$(COOH)_2Cr(CO)_3$ with those of (C_6H_6)$Cr(CO)_3$ (dotted and full lines in Figure 4b), clearly the presence of the carboxylate substituent strongly affect the electronic transitions. In particular, band B shifts from 29100 cm^{-1} to 23400 cm^{-1}, and increases in intensity, with respect to band A. This is in fine agreement with the experimental results and nicely explains why the spectrum of UiO-66/$Cr(CO)_3$ shows a more-intense, better-resolved band at lower frequency, with respect to the spectrum of PS/$Cr(CO)_3$.

3.1.3. Structural and Electronic Properties of PS/Cr(CO)$_3$ Investigated by XAS Spectroscopy. Both FTIR and UV−vis spectroscopies give strong evidence of formation of (arene)$Cr(CO)_3$ species inside the PS and UiO-66 matrices. To have structural confirmation of the nature of the formed species, XAS spectroscopy was performed on the PS/$Cr(CO)_3$ sample. This is a lucky case, since the matrix is highly transparent to the X-ray, and, therefore,

Table 1. Summary of the Structural Parameters Optimized in the Fit of the EXAFS Data for the PS/$Cr(CO)_3$ Sample and for the (η^6-C_6H_6)$Cr(CO)_3$ and $Cr(CO)_6$ Reference Compounds[a]

	$Cr(CO)_6$	(η^6-C_6H_6)$Cr(CO)_3$	PS/$Cr(CO)_3$
$S_0^{2\,b}$	0.8 ± 0.1	1.0 ± 0.1	1
ΔE_0 (eV)[c]	−2 ± 1	−2 ± 1	−4 ± 1
N_{CO}[d]	6	3	2.7 ± 0.6
R_{Cr-CO} (Å)[e]	1.908 ± 0.008	1.850 ± 0.004	1.88 ± 0.01
σ^2_{CO} (Å^2)[f]	0.004 ± 0.001	0.0054 ± 0.0007	0.006 ± 0.002
N_{Bz}[d]	-	6	5.4 ± 1.2
R_{Cr-Bz} (Å)[e]	-	2.220 ± 0.006	2.20 ± 0.03
σ^2_{Bz} (Å^2)[f]	-	0.006 ± 0.001	0.014 ± 0.005
R_{factor}	0.042	0.007	0.042

[a] The fits run in R-space, in the 1.0−3.2 Å range, over a k^3-weighted FT of the $\chi(k)$ functions performed in the 2.0−11.0 Å^{-1} interval. A single S_0^2 and a single ΔE_0 have been optimized for all SS and MS paths. Not optimized parameters are recognizable by the absence of the corresponding error bars. [b] Structural factor (S_0^2); [c] Edge-energy, (ΔE_0), [d] Number of carbonyls (N_{CO}) and of C atoms belonging to the benzene ring (N_{Bz}); [e] Average distance between Cr and the C atoms of carbonyls (R_{Cr-CO}) and between Cr and the C atoms of benzene rings (R_{Cr-Bz}); [f] Debye−Waller factors (σ^2_{CO} and σ^2_{Bz}).

it is possible to get a reasonable signal-to-noise ratio also under highly diluted conditions. It is worth underlining that these data give the first structural evidence of the formation of (arene)$Cr(CO)_3$ species inside a porous matrix. This is also much more important by considering that it is obtained in the case of an amorphous matrix, where XRPD measurements are not informative. Indeed, EXAFS spectroscopy is extremely powerful in defining the local environment around the absorbing atom, independently from the presence of a long-range order. Unfortunately, application of EXAFS was not possible for the UiO-66/$Cr(CO)_3$ system, at least in our experimental conditions, because the matrix is highly absorbing at the Cr K-edge energy,, because of the presence of Zr atoms.

The XANES spectrum of the PS/$Cr(CO)_3$ sample is shown in Figure 5a (black curve) and compared to the spectra of the (η^6-C_6H_6)$Cr(CO)_3$ and $Cr(CO)_6$ reference samples (light gray and dark gray, respectively). All the spectra contain several pre-edge features (A) below the first (B, well-defined peak at 6006 eV) and the second (C, broad component at ∼6025 eV) strong resonances. Resonance B has the highest intensity in each spectrum. The presence of a sharp resonance (B), followed at ∼20 eV by a broader one (C), is typical of the XANES spectra of linear metal carbonyl complexes.[43,63,64] However, it is well-known that the intensity ratio between resonance B and the shape resonance C varies as a function of the number of CO ligands: when going from the octahedral $Cr(CO)_6$ to the pseudo-tetrahedral (η^6-C_6H_6)$Cr(CO)_3$, resonance B becomes weaker and resonance C is broadened.[65] Therefore, in a first approximation, it is possible to deduce the number of carbonyl ligands characterizing the species formed in the PS matrix by looking at the relative ratio between the two resonances. Additionally, the intensity of the pre-edge features increases by going from perfect octahedral complexes to pseudo-tetrahedral ones. The pre-edge features are assigned to the $A_{1g} \rightarrow T_{2g}$ and $A_{1g} \rightarrow E_g$ transitions, which are dipole-forbidden in a perfect octahedral case but become allowed when the symmetry is lowered.[44,66,67] Coming in more details, $Cr(CO)_6$ presents two weak pre-edge bands at 5993 and 5997 eV, whereas (η^6-C_6H_6)$Cr(CO)_3$ is characterized by a sharp and quite intense band at 5991 eV with a shoulder at 5993 eV, and by a weaker component at 5996 eV, which appears overlapped to the sharp white line feature. It is evident that a careful comparison of the pre-edge region could give important information on the local structure around Cr in the complex formed inside PS.

The XANES spectrum of the PS/$Cr(CO)_3$ sample is very similar to that of the (η^6-C_6H_6)$Cr(CO)_3$ reference, as evidenced especially by the derivative signal (bottom part in Figure 5a), with the following exceptions: (i) unless at the same energy position, the pre-edge features are less intense; (ii) feature B is less intense; (iii) the shape resonance C is slightly different. These features suggest that the complexes formed inside PS are characterized by a coordination geometry slightly different, with respect to the bare complex in the solid state. In particular, it has been pointed out that resonance C contains information on the bond length between Cr and C atoms of the carbonyl ligands.[65] Therefore, a change in this region suggests a difference in the geometry of the carbonyl ligands around Cr by going from (η^6-C_6H_6)$Cr(CO)_3$ to PS/$Cr(CO)_3$. These differences, qualitatively predicted from XANES spectra, will be quantitatively estimated by fitting the EXAFS data.

The k^3-weighted, phase-uncorrected FT of the EXAFS functions for PS/$Cr(CO)_3$ is reported in Figures 5b and 5c, in both modulus and imaginary parts, and compared to those of the reference compounds. Clear differences in the coordination shell of Cr are observed. The |FT| of $Cr(CO)_6$ (the top part of Figure 5b) is dominated by two peaks, centered at 1.4 and 2.4 Å (without phase correction), which correspond to the first shell Cr−C and second shell Cr−O contributions of the six carbonyl ligands, respectively. Note that the second shell peak is

(63) Lamberti, C.; Palomino, G. T.; Bordiga, S.; Berlier, G.; D'Acapito, F.; Zecchina, A. *Angew. Chem., Int. Ed.* **2000**, *39*, 2138–2141.
(64) Prestipino, C.; Capello, L.; D'Acapito, F.; Lamberti, C. *Phys. Chem. Chem. Phys.* **2005**, *7*, 1743–1746.
(65) Engemann, C.; Hormes, J.; Longen, A.; Dotz, K. H. *Chem. Phys.* **1998**, *237*, 471–481.
(66) Bordiga, S.; Coluccia, S.; Lamberti, C.; Marchese, L.; Zecchina, A.; Boscherini, F.; Buffa, F.; Genoni, F.; Leofanti, G.; Petrini, G.; Vlaic, G. *J. Phys. Chem.* **1994**, *98*, 4125–4132.
(67) Groppo, E.; Lamberti, C.; Spoto, G.; Bordiga, S.; Magnacca, G.; Zecchina, A. *J. Catal.* **2005**, *236*, 233–244.

very high in intensity, because of the important contributions of the collinear Cr−C−O MS paths, enhanced by focusing effect.[63,64,68] The results of the data analysis (see the first column in Table 1 and full line in the top part of Figures 5b and 5c) are in agreement with the structural data obtained by XRD. A completely different signal is obtained in the case of (η^6-C_6H_6)$Cr(CO)_3$ (the middle part of Figures 5b and 5c). In this case, the |FT| is still dominated by two main components; however, while the second one occurs almost at the same position as that found for $Cr(CO)_6$, the first one is clearly doubled and shifted in distance. This is due to the fact that the first coordination shell around Cr is composed of three carbonyl ligands (dotted curve) and six C atoms belonging to the benzene ring (dashed curve), at a slightly different distance (see the second column in Table 1). This results in an apparent shift of the first shell component toward higher distances, with respect to the $Cr(CO)_6$ sample.

As far as PS/$Cr(CO)_3$ is considered, the |FT| spectrum (the bottom part of Figure 5b) is completely different from the spectra of both reference compounds, being characterized by three peaks, the first two with an overall intensity that is around half of that shown by the first shell signal of both $Cr(CO)_6$ and (η^6-C_6H_6)$Cr(CO)_3$. Actually, the three peaks arise from the combination of the two first shell signals coming from the CO ligands (dotted curve) and the benzene ring (dashed curve), respectively. In this case, both the $Cr-C_{Bz}$ and $Cr-C_{CO}$ distances are slighlty modified, with respect to the (η^6-C_6H_6)$Cr(CO)_3$ reference compound, so that they are now almost opposite in phase (see imaginary parts in the bottom part of Figure 5c). This phenomenon is the main responsible for the decrease in intensity of the overall signal (since part of the signal is canceled by the negative interpherence between the first-shell signals). The data analysis results in 2.7 ± 0.6 carbonyl ligands at an average distance (R_{Cr-CO}) of 1.88 ± 0.01 Å, and 5.4 ± 1.2 carbons of the arene ring at an average distance (R_{Cr-Bz}) of 2.220 ± 0.006 Å (see the third column in Table 1). The Debye−Waller factor obtained for the arene ligand (0.016 ± 0.005 Å^2) is indicative of a certain degree of heterogeneity; this is expected, because the arene rings belong to the flexible and heterogeneous PS matrix. The small differences in the relative distance of Cr notwithstanding, with respect to the CO and arene ligands, EXAFS spectroscopy definitely proves, also from a structural point of view, that the species formed inside PS are of the type (arene)$Cr(CO)_3$. The small geometrical differences and the higher heterogeneity (Debye−Waller values), with respect to the structure of the bare compound in the solid state, could be responsible for the differences observed in the UV−vis spectra between the PS/$Cr(CO)_3$ sample and the (η^6-C_6H_6)$Cr(CO)_3$ reference compound.

3.2. Photoreaction of UiO-66/$Cr(CO)_3$. Photochemistry of organometallic (η^6-arene)$M(CO)_3$ complexes has been

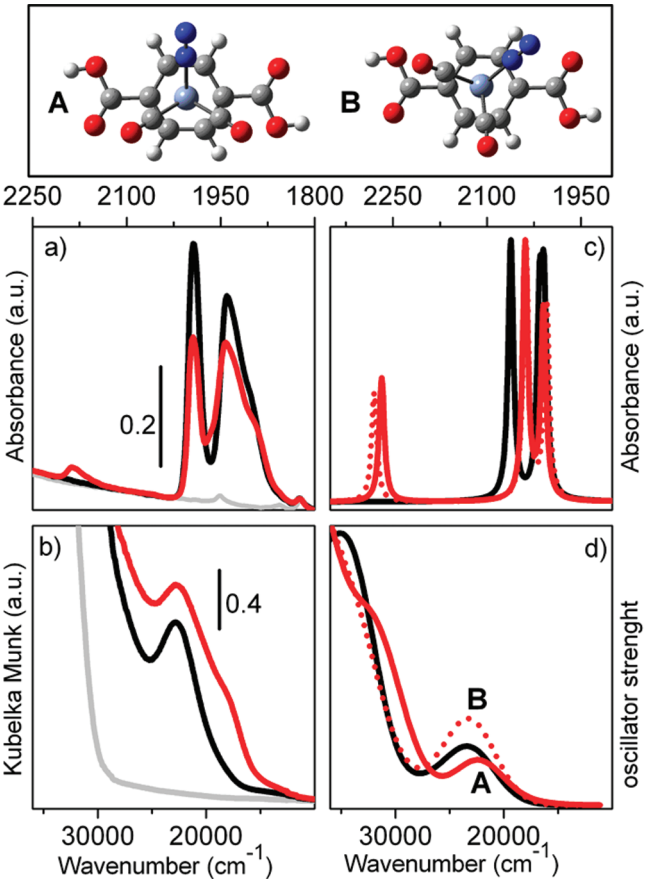

Figure 6. (a) Evolution of the FT-IR spectrum of UiO-66/$Cr(CO)_3$ (black) upon photoirradiation under N_2 atmosphere (red) for 5 min. The spectrum of UiO-66 before functionalization is reported in gray. (b) Same experiments followed by UV−vis spectroscopy. (c and d) Simulated IR and optical spectra for (C_6H_4)$(COOH)_2Cr(CO)_3$ (black) and for the two conformers of (C_6H_4)$(COOH)_2Cr(CO)_2(N_2)$ (full and dotted red lines for conformer A and B, respectively).

extensively studied in solution,[27,69] matrix isolation,[34,70] supercritical fluids,[29] and polymeric matrices.[24,30] Photoactive organometallic compounds adsorbed or supported on high-surface-area porous supports could serve as important gas storage media (in particular, H_2)[71] and also as active catalyst sites (photocatalytic hydrogenation of dienes),[72−74] if present in sufficient concentration, well-dispersed, and in chemically accessible form. Depending on the photolysis condition, one or more CO can be removed, to produce coordinatively unsaturated metal subcarbonyls or even metal atoms.[70,75−78] Moreover, it

(68) Filipponi, A.; Dicicco, A.; Zanoni, R.; Bellatreccia, M.; Sessa, V.; Dossi, C.; Psaro, R. *Chem. Phys. Lett.* **1991**, *184*, 485–490.
(69) Simon, J. D.; Xie, X. *J. Phys. Chem.* **1986**, *90*, 6751–6753.
(70) Bloyce, P. E.; Hooker, R. H.; Rest, A. J.; Bitterwolf, T. E.; Fitzpatrick, N. J.; Shade, J. E. *J. Chem. Soc., Dalton Trans.* **1990**, 833–841.
(71) Cooper, A. I.; Poliakoff, M. *Chem. Commun.* **2007**, 2965–2967.
(72) Clarke, M. J.; Cooper, A. I.; Howdle, S. M.; Poliakoff, M. *J. Am. Chem. Soc.* **2000**, *122*, 2523–2531.
(73) Jackson, S. A.; Hodges, P. M.; Poliakoff, M.; Turner, J. J.; Grevels, F. W. *J. Am. Chem. Soc.* **1990**, *112*, 1221–1233.
(74) Childs, G. I.; Cooper, A. I.; Nolan, T. F.; Carrott, M. J.; George, M. W.; Poliakoff, M. *J. Am. Chem. Soc.* **2001**, *123*, 6857–6866.
(75) Brecknridge, W. H.; N., S. *J. Phys. Chem.* **1981**, *85*, 3557–3560.
(76) Tumas, W.; Gitlin, B.; Rosan, A. M.; Yardley, J. T. *J. Am. Chem. Soc.* **1982**, *140*, 55–59.
(77) Fletcher, T. R.; Rosenfeld, R. N. *J. Am. Chem. Soc.* **1983**, *105*, 6358–6359.
(78) Seder, T. A.; Church, S. P.; Ouderkirk, A. J.; Writz, E. *J. Am. Chem. Soc.* **1985**, *107*, 1432–1433.

has been also demonstrated that such systems undergo light-activated substitution chemistry, in which CO ligand is replaced by N_2 and H_2.[29,31,70,79] Recently, Kaye et al.[23] have shown that the $Cr(CO)_3$ moieties anchored on benzene ring of MOF-5 undergo analogous photochemical reaction when irradiated with a 450-nm laser.

Here, we made a similar attempt on UiO-66. After functionalization, UiO-66/$Cr(CO)_3$ has been exposed to UV light in a N_2 atmosphere for increasing time. The occurrence of light-activated substitution of one CO ligand with a N_2 molecule has been followed by both FT-IR and UV−vis spectroscopies (see Figure 6). A few minutes of UV irradiation are sufficient to cause relevant modifications in both FT-IR and UV−vis spectra. In the FT-IR spectra (Figure 6a), the two bands centered at 1998 and 1944 cm^{-1} characterizing the (arene)$Cr(CO)_3$ species (black spectrum) decrease in intensity, with the attendant formation of a weak and broad band at 2187 cm^{-1} (red spectrum), which is easily assigned to the ν(NN) stretching of coordinated N_2, demonstrating the formation of the UiO-66/$Cr(CO)_2(N_2)$ mixed complex. In addition, a small absorption appears in the region between the main ν(CO) bands, accompanied by a shoulder at ~1901 cm^{-1}. The obtained spectrum is very similar to that reported in the literature for $Zn_4O[(BDC)Cr(CO)_2(N_2)]_3$[23] and $(C_6H_6)Cr(CO)_2(N_2)$,[29] and it well agrees with the changes expected on the basis of theoretical calculations performed on two possible conformers of $C_6H_4(COOH)_2Cr(CO)_2N_2$ (Figure 6c). Note that only a small fraction of $Cr(CO)_3$ are interested by the substitution, mainly because the experiment is conducted under static conditions.

Finally, exposure times longer than 30 min lead to the decomposition of the (arene)$Cr(CO)_3$ species, as testified by the disappearance of the vibrational bands in both the ν(CO) and ν(NN) regions (spectra not reported). The same occurs on the PS/$Cr(CO)_3$ sample after very short irradiation times, suggesting a higher lability of the complex under UV irradiation (spectra not reported).

The light-activated CO substitution by N_2 in UiO-66/$Cr(CO)_3$ is also demonstrated by the changes in the UV−vis spectrum (see Figure 6b). After irradiation for a few minutes, the sample slightly changes in color; as a consequence, the overall intensity of the UV−vis spectrum increases and a new band at 18 450 cm^{-1} appears. These changes are nicely predicted by theoretical calculations performed on two possible conformers of $C_6H_4(COOH)_2Cr(CO)_2N_2$ (see Figure 6d). In the case of conformer A (full red line in Figure 6d), the simulated electronic transitions are red-shifted, with respect to $C_6H_4(COOH)_2Cr(CO)_3$ (black line), whereas for conformer B, an increase in intensity is observed (dotted red line). The experimental spectrum obtained for UiO-66/$Cr(CO)_2(N_2)$ can be explained in terms of the copresence of both conformers, thus explaining both the increase of the overall intensity and the appearance of a band at lower frequency, with respect to the starting spectrum.

(79) Walsh, E. F.; George, M. W.; Goff, S.; Nikiforov, S. M.; Popov, V. K.; Sun, X. Z.; Poliakoff, M. *J. Phys. Chem.* **1996**, *100*, 19425–19429.

4. Conclusions

Two highly porous matrices (UiO-66 and PS), whose structure is characterized by the presence of differently substituted benzene rings, have been successfully functionalized by grafting $Cr(CO)_3$ species, following the thermal decomposition of $Cr(CO)_6$ precursor. UiO-66 is a cubic close-packed three-dimensional metal−organic framework composed by a zirconia-based inorganic building brick and 1,4-benzene dicarboxylic acid as organic linker, where the Zr sites do not present any coordination vacancy. PS is a commercial poly(ethyl-co-divinylbenzene), with a surface area and porosity very similar to those of UiO-66. The vibrational, electronic, and structural properties of the grafted $Cr(CO)_3$ species have been completely investigated by means of FT-IR, UV−vis, XANES, and EXAFS spectroscopies, complemented by theoretical calculations. It is definitely demonstrated that the nature of the benzene ring substituent (a carboxylate or a CH_2 group, respectively) influences the final properties of the functionalized matrix, as previously predicted by theoretical calculation.[36] In the case of UiO-66/$Cr(CO)_3$ material, the photoinduced substitution of one CO ligand with a N_2 molecule under UV irradiation also has been explored.

The functionalization of highly porous, hybrid, or completely organic matrices (either crystalline or amorphous in nature) with $Cr(CO)_3$ species opens interesting perspective in the field of heterogeneous catalysis and organometallic chemistry, as well as the storage of small molecules. Therefore, the data reported here could be of interest for a wide scientific community, and suggest a systematic procedure to investigate the functionalization process of porous matrices.

Acknowledgment. Prof. A. Zecchina is kindly acknowledged for fruitful discussion. The entire staff of BM26A (and, in particular, S. Nikitenko) are gratefully acknowledged for the help provided during the XAS measurements. This work is part of the STREP Project MOFCAT (under Contract No. NMP4-CT-2006-033335).

Supporting Information Available: XRPD patterns, and corresponding Rietveld refinements; detailed description of the EXAFS data analysis; IR and UV spectra demonstrating the formation of (arene)$Mo(CO)_3$ complex. (PDF) This material is available free of charge via the Internet at http://pubs.acs.org.